Eur. Phys. J. C 50, 341–352 (2007)
DOI 10.1140/epjc/s10052-007-0260-4

THE EUROPEAN PHYSICAL JOURNAL C

Regular Article – Experimental Physics

Multiplicity studies and effective energy in ALICE at the LHC

In memory of A. Smirnitskiy[1]

A. Akindinov[1], A. Alici[2,3], P. Antonioli[3], S. Arcelli[2,3], M. Basile[2,3], G. Cara Romeo[3], M. Chumakov[1], L. Cifarelli[2,3,a], F. Cindolo[3], A. De Caro[5], D. De Gruttola[5], S. De Pasquale[5], M. Fusco Girard[5], C. Guarnaccia[5], D. Hatzifotiadou[3], H.T. Jung[6], W.W. Jung[6], D.W. Kim[6], H.N. Kim[6], J.S. Kim[6,7], S. Kiselev[1], G. Laurenti[3], K. Lee[6], S.C. Lee[6], E. Lioublev[1], M.L. Luvisetto[3], A. Margotti[3], A. Martemiyanov[1], R. Nania[3], F. Noferini[2,3,4], P. Pagano[5], A. Pesci[3], R. Preghenella[2,3], G. Russo[5], E. Scapparone[3], G. Scioli[2,3], R. Silvestri[5], Y. Sun[7], I. Vetlitskiy[1], K. Voloshin[1], L. Vorobiev[1], M.C.S. Williams[3], B. Zagreev[1], C. Zampolli[2,3,4], A. Zichichi[2,3,4]

[1] Institute for Theoretical and Experimental Physics, Moscow, Russia
[2] Dipartimento di Fisica dell'Università, Bologna, Italy
[3] Sezione INFN, Bologna, Italy
[4] Museo Storico della Fisica e Centro Studi e Ricerche "Enrico Fermi", Rome, Italy
[5] Dipartimento di Fisica dell'Università and INFN, Salerno, Italy
[6] Department of Physics, Kangnung National University, Kangnung, South Korea
[7] World Laboratory, Lausanne, Switzerland

Received: 30 October 2006 / Revised version: 12 February 2007 /
Published online: 13 March 2007 –

Abstract. In this work we explore the possibility to perform "effective energy" studies in very high energy collisions at the CERN large hadron collider (LHC). In particular, we focus on the possibility to measure in *pp* collisions the average charged multiplicity as a function of the effective energy with the ALICE experiment, using its capability to measure the energy of the leading baryons with the zero degree calorimeters. Analyses of this kind have been done at lower centre-of-mass energies and have shown that, once the appropriate kinematic variables are chosen, particle production is characterized by universal properties: no matter the nature of the interacting particles, the final states have identical features. Assuming that this universality picture can be extended to *ion–ion* collisions, as suggested by recent results from RHIC experiments, a novel approach based on the scaling hypothesis for limiting fragmentation has been used to derive the expected charged event multiplicity in *AA* interactions at LHC. This leads to scenarios where the multiplicity is significantly lower compared to most of the predictions from the models currently used to describe high energy *AA* collisions. A mean charged multiplicity of about 1000–2000 per rapidity unit (at $\eta \sim 0$) is expected for the most central Pb–Pb collisions at $\sqrt{s_{\mathrm{NN}}} = 5.5$ TeV.

1 Introduction

In high-energy particle collisions, bulk event properties like the average charged particle multiplicity are regarded as experimental observables of fundamental interest, providing important information on the dynamics of the interaction. In particular, the average charged particle multiplicity in multihadronic final states has so far been measured in many different interaction systems (e^+e^- and $pp(\bar{p})$ collisions, DIS processes, etc.) and over a wide range of centre-of-mass energies. Although the data show a dependence on $\sqrt{s}$ which is characteristic of the specific initial state under consideration, as pointed out in [1–6] a universal behaviour can actually be identified if the appropriate definition of the energy available for particle production (the "effective energy") is used.

The aim of this work is to address the possibility to perform an effective energy study at energies of several TeV at LHC, with the ALICE experiment [7–9]. With this respect ALICE (a large ion collider experiment) has an excellent capability, thanks to the presence of several detectors for the measurement of the particle multiplicity over a wide rapidity range [10, 11]. Moreover, on both sides of the beam interaction point, the detector will be equipped with very forward calorimeters, the zero degree calorimeters (ZDCs) [12], which will allow to derive the effective energy on an event-by-event basis by measuring the energy of the leading nucleons.

This paper is organized as follows. In Sect. 2 we briefly review the main experimental results which support the existence of a universal behaviour in particle production, independently of the nature of the colliding system. In Sect. 3 a simplified analysis based on the PYTHIA Monte Carlo is presented, showing that this event genera-

[a] e-mail: Luisa.Cifarelli@bo.infn.it

tor is able to reproduce to a good extent the experimental observations described in Sect. 2, and can therefore be used to evaluate the feasibility of an effective energy study at the LHC energies. A more detailed analysis is then described in Sect. 4, where the capability of the ALICE detector to measure the energy of the leading baryons in pp collisions at the LHC is quantified using a realistic simulation of the ALICE ZDC detector response. Finally, in Sect. 5 we present a prediction for the total charged multiplicity in Pb–Pb interactions at LHC, assuming that the universality features discussed herein hold also for ultrarelativistic heavy ion collisions.

2 What we learned from previous experiments

It is well known that the average charged multiplicity in e^+e^- collisions follows a logarithmic dependence on the centre-of-mass energy $\sqrt{s}$. Figure 1 shows a compilation of data from e^+e^- experiments [13–29] over a wide range of centre-of-mass energies (full black symbols), together with the result of a logarithmic fit to the measurements, indicated by the dashed line. As mentioned in Sect. 1, the average charged multiplicity is characterized by a significantly different dependence on $\sqrt{s}$ if other initial states are considered. In particular, in the case of $pp(\bar{p})$ collisions the charged particle multiplicity at a fixed centre-of-mass energy is observed to be systematically lower than what can be inferred from the e^+e^- data at the same $\sqrt{s}$ (see again Fig. 1, open symbols, data from [30–38]). As pointed out in [1–4], this behaviour can be understood after considering that, while in e^+e^- collisions the energy available for particle production coincides with the full centre-of-mass energy (once the effects from the initial state radiation are removed), in $pp(\bar{p})$ collisions this energy is reduced with respect to $\sqrt{s}$ due to a basic feature of the hadronic interactions, the "leading effect".

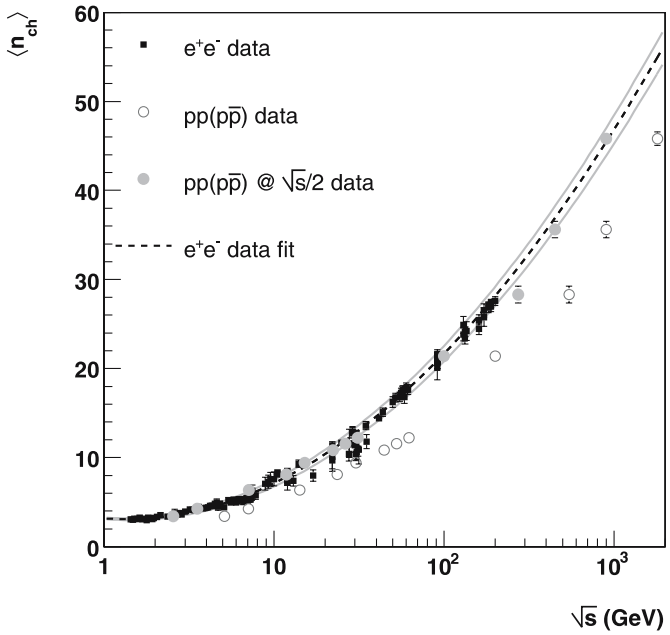

Fig. 1. Average charged particle multiplicity measured in e^+e^- (*full black symbols*) and $pp(\bar{p})$ (*open symbols*) collisions. A logarithmic fit to the e^+e^- data is also shown as the *dashed line*. The *full grey symbols* indicate the $pp(\bar{p})$ data after the centre-of-mass energies have been scaled by a factor $\frac{1}{2}$ (see text)

The leading effect, which is related to the quantum number flow between the initial and the final state, implies that in $pp(\bar{p})$ collisions there is a high probability to emit a forward baryon with large longitudinal momentum along the direction of the incident beams. Since the leading baryon carries away a fraction of the incident energy, the energy available for particle production is reduced with respect to the total centre-of-mass energy. If the leading effect is taken into account in the definition of the effective energy available for particle production, $E_{\rm eff}$, common universal features can be observed in the two different interaction systems, e^+e^- and $pp(\bar{p})$.

In particular, as done in [6], the effective energy can be estimated on an event-by-event basis by measuring the energy $E_{\rm leading}$ of the leading baryon in each event hemisphere (the hemispheres being defined with respect to a plane transverse to the direction of the incident beams in the centre-of-mass system). The effective energy per hemisphere $(E_{\rm eff})_i$ is then given by:

$$(E_{\rm eff})_i = \sqrt{s}/2 - (E_{\rm leading})_i \quad \text{for} \quad i = 1, 2\,. \tag{1}$$

Notice that, by measuring the energy of the leading particles event by event, a wide range of effective energies can be covered at a fixed centre-of-mass energy. Relying on the experimental observation of the independence of the two event hemispheres with respect to the leading effect [6], the total effective energy $E_{\rm eff}$ available for particle production in the whole event can be derived from the measurement of only one leading particle per event, using the relation:

$$E_{\rm eff} = 2(E_{\rm eff})_i = \sqrt{s} - 2(E_{\rm leading})_i\,. \tag{2}$$

Correspondingly, the average total charged multiplicity in the event is given by:

$$\langle n_{\rm ch} \rangle = 2\,\langle n_{\rm ch} \rangle_i\ . \tag{3}$$

Alternatively, in those events where a leading particle is measured in both hemispheres, the total effective energy can also be derived from the relation:

$$E_{\rm eff} = \sqrt{s[1-(x_{\rm F})_1][1-(x_{\rm F})_2]}\,, \tag{4}$$

where $(x_{\rm F})_i$ are the measured Feynman–x of the two leading nucleons, $(x_{\rm F})_i = 2\,(p_L)_i/\sqrt{s}$.

The two methods of defining the effective energy in the event have been proved to be equivalent, as shown in [1–4]; it should be noticed, however, that the first one has the advantage of making optimal use of the data in terms of the collected event statistics, obviously owing to the much larger acceptance and efficiency of single with respect to double leading particle detection.

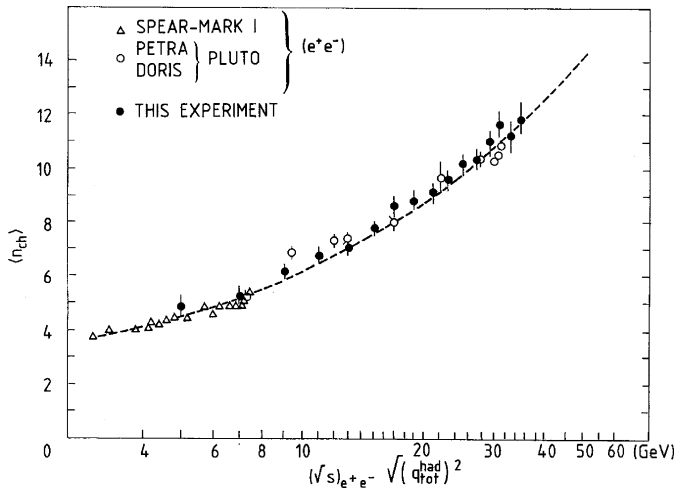

Fig. 2. Average charged multiplicity $\langle n_{\rm ch}\rangle$ as a function of the effective energy $E_{\rm eff}$ (here indicated as $\sqrt{(q_{\rm tot}^{\rm had})^2}$), as measured in minimum bias pp collisions collected by the SFM experiment at the CERN ISR (*full circles*). The data from e^+e^- experiments are also shown (*open circles* and *triangles*) in terms of $\sqrt{s}$. A fit to ISR–pp data is superimposed. The plot is taken from [5]

As mentioned before, after taking into account the leading effect and using the effective energy instead of the full centre-of-mass energy, a very good agreement between the measured charged particle multiplicity in e^+e^- and pp collisions is obtained, as shown in Fig. 2. The pp data in this figure refer to a "minimum bias" event sample from which elastic and diffractive processes were excluded, with leading protons in the range $0.3 \lesssim x_{\rm F} \lesssim 0.8$ (see later on Sects. 3 and 4).

A good agreement between the inclusive $pp(\bar{p})$ results presented in Fig. 1 and e^+e^- results is also obtained if the $pp(\bar{p})$ centre-of-mass energies are scaled by a factor $\frac{1}{2}$ (full grey symbols). This is a direct consequence of the effective energy being the relevant variable in particle production, and of the assumption, supported by several measurements [1–4], that the Feynman–x distribution of the leading particles has a mean value equal to ~ 0.5, resulting in an average effective energy which is about half the full centre-of-mass energy.

3 Pythia simulations

The PYTHIA6.214 [39] Monte Carlo has been used to simulate pp collisions at a centre-of-mass energy of 14 TeV. An effective energy study carried on for pp collisions requires a precise definition of the type of events to be used. Following the choice of the original ISR–pp experiment [1–6], only non diffractive minimum bias events have been considered herein. It should be noted that most of the other $pp(\bar{p})$ experiments [30–38] quoted in Sect. 2 included double-diffractive processes in their definition of minimum bias. With PYTHIA the double-diffraction contribution is at the level of 15% with respect to the non diffractive one at $\sqrt{s} = 14$ TeV (using default generation parameters). A brief description of the ALICE pp minimum bias trigger capabilities for both diffractive and non diffractive processes is given in Sect. 4.1.

To optimize the agreement with respect to the dependence observed in the data for the charged particle multiplicity as a function of the effective energy, some of the PYTHIA parameters regulating the treatment of the multiple parton interactions (MI) have been tuned. This MI model has been introduced and widely discussed in the literature [40–43] in order to describe the basic features and, in particular, the charged particle multiplicity of high energy minimum bias $pp(\bar{p})$ final states up to $\sqrt{s} \sim 1$ TeV. It is still under investigation but represents however one possible tool to perform extrapolations in the multi-TeV domain at LHC. The set of values used in the simulation is reported in Table 1.

Notice that the only three parameters tuned correspond, respectively, to the selection of the MI mechanism features in terms of hadronic matter distribution (MSTP(82)), the regularization scale of the transverse momentum spectrum of the process (PARP(82)) which controls the MI rate and the exponent of the $\sqrt{s}$-power law dependence of the MI mechanism (PARP(90)) [39].

Figure 3 shows the mean total charged multiplicity for generated pp collisions over a wide range of centre-of-mass energies, with $\sqrt{s}$ rescaled by a factor $\frac{1}{2}$ to take into account, on average, the energy carried away by the leading nucleons, as done in Sect. 2. To derive the average charged multiplicity $\langle n_{\rm ch}\rangle$ all primary charged particles in the event (including the decay products of short-lived resonances) with no transverse momentum cutoff and in the full angular acceptance have been considered. Although $\langle n_{\rm ch}\rangle$ is derived from the Monte Carlo information at the event generator level, notice that the ALICE detector is expected to measure the multiplicity with a good accuracy, high efficiency and over a wide acceptance both in case of pp and Pb–Pb collisions (as reported in chapter 6.1.5 of [11]).

Using the tuned PYTHIA Monte Carlo, a very good agreement with the fit that describes the $\sqrt{s}$ dependence of the multiplicity for e^+e^- collisions (see Fig. 1) is observed in Fig. 3 over the whole range of energies. Using instead the default values, PYTHIA disagrees by $\sim 10\%$ with the e^+e^- fit for $\sqrt{s} > 1$ TeV.

Table 1. Values of the PYTHIA parameters tuned for this work to generate minimum bias (non diffractive) pp events at various centre-of-mass energies

Parameter	Our tuning	Default
MSTP(51)	7 (CTEQ5L)	7 (CTEQ5L)
MSTP(81)	1	1
MSTP(82)	2	4
PARP(82)	2.15 GeV	1.80 GeV
PARP(89)	1000 GeV	1000 GeV
PARP(90)	0.215	0.160

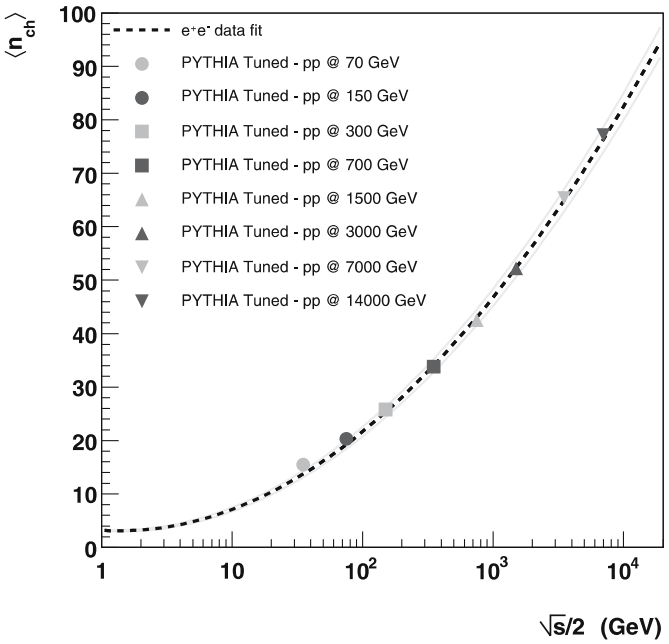

Fig. 3. Mean charged multiplicity $\langle n_{\rm ch} \rangle$ in pp collisions from PYTHIA Monte Carlo, at $\sqrt{s} = 70$ to 14 000 GeV. The energy on the horizontal axis is scaled by a factor $\frac{1}{2}$ in order to take into account an average leading effect in the pp final states. The e^+e^- fit of Fig. 1 is also plotted

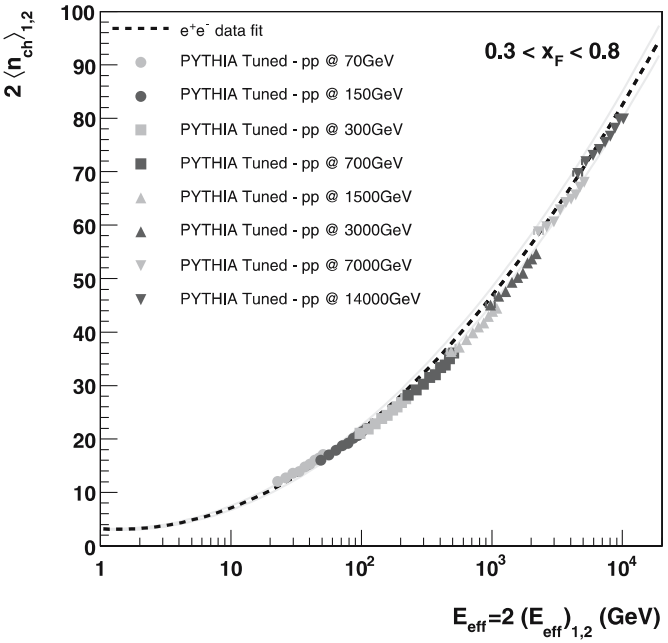

Fig. 4. Mean charged multiplicty $\langle n_{\rm ch} \rangle$ in pp PYTHIA events at $\sqrt{s} = 70$ to 14 000 GeV with respect to effective energy. The e^+e^- fit is also plotted. Here the single hemisphere variables are considered and scaled by a factor of 2 (see text)

A satisfactory agreement is also observed when studying the multiplicity as a function of the effective energy in each single event. Following the approach described in Sect. 2, for each event the effective energy in a single hemisphere was derived from the energy of the corresponding leading baryon (defined as the highest longitudinal momentum baryon in the hemisphere) and then multiplied by 2, according to relation (2). The total charged multiplicity was also derived on a single hemisphere basis, scaled by the same factor of 2. As can be seen from Fig. 4, also in this case the dependence of the total charged multiplicity on the effective energy follows closely[1] the fit to the e^+e^- data.

Notice that in the above analysis the Feynman-x of the leading baryons was restricted to be in the range: $0.3 < x_{\rm F} < 0.8$. The lower cutoff, $x_{\rm F}^{\rm min} = 0.3$, is mainly motivated by the fact that in a realistic analysis the identity of the leading particle will not be accessible. Some care is therefore required in defining an appropriate Feynman-x acceptance, in order to ensure that the energy measured in the forward region is indeed in most cases due to a leading baryon, and that the contamination from leading particles which are not baryons is kept below a reasonably small level. In Fig. 5 the $x_{\rm F}$ distribution of the leading baryon, defined as the proton/neutron with the highest longitudinal momentum (i.e. with the highest Feynman-x $x_{\rm F} = 2p_L/\sqrt{s}$) among all baryons produced in a given event hemisphere, is shown as the dark-shaded histogram, for 10^5 pp collisions generated at $\sqrt{s} = 14$ TeV. The $x_{\rm F}$ distribution for the cases where this leading nucleon is also the leading particle among all particles (baryons or non

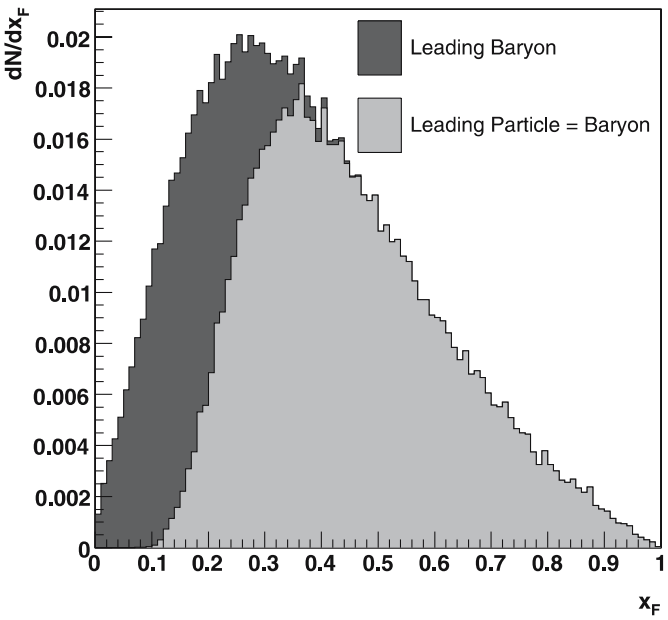

Fig. 5. The $x_{\rm F}$ distribution of the most energetic baryon (*dark-shaded histogram*) in each hemisphere for pp collisions at $\sqrt{s} =$ 14 TeV. The $x_{\rm F}$ distribution of this baryon in the case it is also the most energetic particle in the hemisphere is shown as the *light-shaded histogram*

[1] The values deviate systematically from the e^+e^- data fit as $E_{\rm eff}$ increases whereas they always start well on the fit line. This effect is likely due to the fact that the multiple interaction parametrization of PYTHIA generator slightly depends also on the centre-of-mass energy.

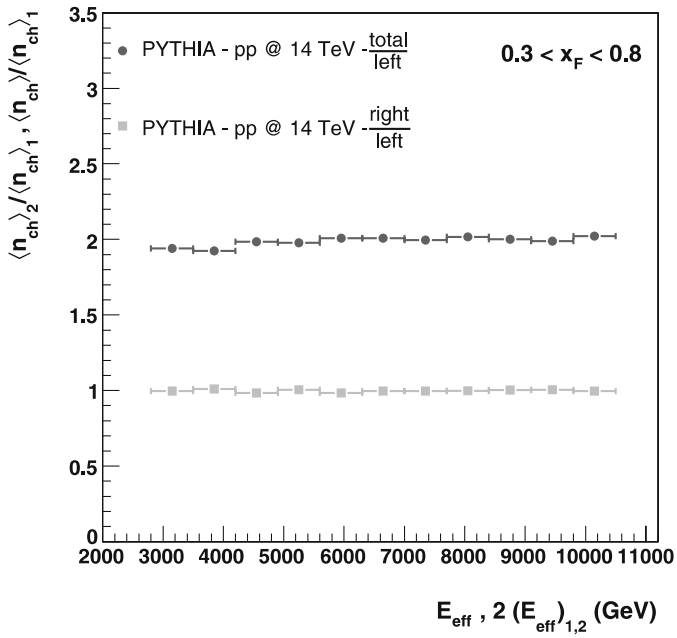

Fig. 6. Average charged multiplicity ratio $\langle n_{\rm ch}\rangle / \langle n_{\rm ch}\rangle_1$ as a function of the total effective energy $E_{\rm eff}$ (*black symbols*) and average charged multiplicity ratio $\langle n_{\rm ch}\rangle_2 / \langle n_{\rm ch}\rangle_1$ as a function of the effective energy in a single hemisphere scaled by a factor 2, $E_{\rm eff} = 2(E_{\rm eff})_{1,2}$ (*grey symbols*)

baryons) of the same hemisphere is superimposed as the light-shaded histogram. For Feynman-x greater than 0.3, it can be seen that the leading nucleon is indeed the leading particle in the event hemisphere. Moreover, a request of a minimum $x_{\rm F}$ allows to reduce the contamination from leading particles that are not baryons. At $x_{\rm F} = 0.3$ this contamination is $\sim 30\%$ and rapidly decreases for $x_{\rm F} > 0.3$.

For what concerns the constraint on the maximum $x_{\rm F}$, the requirement $x_{\rm F}^{\rm max} = 0.8$ was ispired by the original effective energy data analysis [1–6], where the same kind of cutoff on leading protons was imposed. This $x_{\rm F} < 0.8$ condition, which fairly matches the acceptance of the ALICE ZDC calorimeters for leading baryons (see later on Sect. 4), would also imply the rejection of the proton[2] single-diffraction peak (not considered in this study).

The PYTHIA generator reproduces to a good extent also other features related to the leading effect which have been observed in the data. As an example, Fig. 6 shows, for pp collisions at $\sqrt{s} = 14\,\text{TeV}$, the ratio between the total charged multiplicity $\langle n_{\rm ch}\rangle$, measured as a function of the total effective energy $E_{\rm eff}$ given by equation (4), and the average charged multiplicity in a single hemisphere, measured as a function of the effective energy in a single hemisphere, scaled by a factor 2, $E_{\rm eff} = 2(E_{\rm eff})_{1,2}$. The ratio is consistent with the relation $\langle n_{\rm ch}\rangle = 2\,\langle n_{\rm ch}\rangle_{1,2}$ in agreement with the hypothesis of the two event hemispheres being independent with respect to the leading effect, and of the equivalence of the two effective energy $E_{\rm eff}$ definitions presented in Sect. 2, (2) and (4).

[2] For neutrons single-diffraction processes with charge exchange are highly unlike.

4 Tagging of leading nucleons with the ALICE ZDC detector in pp collisions

Although the programme of the ALICE experiment has its main focus on heavy ion physics, the detector will also have excellent physics capabilities in the case of pp collisions. In particular, this applies to the analysis we are presenting in this paper.

4.1 ALICE performance for the selection and measurement of pp events

A detailed description of the ALICE trigger system can be found elsewhere [11, 44]. Here we will limit ourselves to a brief report on both the minimum bias trigger selection and the charged particle multiplicity measurement [11] that ALICE will be able to perform in pp collisions at LHC.

The minimum bias trigger is realized coupling different signals coming from the V0 [45] and the SPD [46] detectors. The general purpose of this minimum bias trigger is to select events from pp collisions with an efficiency as high as possible, and a bias as low as possible, and to reject events due to beam-gas or beam-halo. The V0 is made up of two different arrays of scintillators placed along the beam pipe in the forward/backward directions. It provides two kinds of signals: (i) VZERO.OR that requires at least one hit in one counter on one side and (ii) VZERO.AND that requires at least one hit in one counter on both sides. The SPD (silicon pixel detector) is made up of two coaxial layers of silicon sensors which also provide a trigger signal (GLOB.FO) consisting in a fast-OR signal of all its 1200 chips (400 in the inner layer, 800 in the external one). Different combinations of these signals, coupled to a non background trigger (notBG, defined by requiring no signals in either of the V0 counters within appropriate time windows corresponding to beam-background processes), set different trigger configurations. The three configurations

Table 2. Signal configurations for pp minimum bias trigger

MB 1	GLOB.FO	or	VZERO.OR	and	notBG
MB 2	GLOB.FO	and	VZERO.OR	and	notBG
MB 3	GLOB.FO	and	VZERO.AND	and	notBG

Table 3. Minimum bias trigger efficiency for different (diffractive and non diffractive) pp processes

Process ($\sigma_{14\,\text{TeV}}$ [mb])	MB1 (%)	MB2 (%)	MB3 (%)
Non Diff. (55.22)	99.9	99.1	96.9
Single-Diff. (14.30)	73.8	59.5	38.4
Double-Diff. (9.78)	87.8	68.7	45.6

are listed in Table 2, while the corresponding efficiencies are reported in Table 3.

The multiplicity can be measured counting the "tracklets" (extracted by the association of the signals in both the two layers of the SPD) with the SPD in the central region and with the FMD (forward multiplicity detector) [45] in the forward region. The pseudorapidity range covered by the ALICE detector is about 8 η-units. In this range an accurancy on the multiplicity better than 10% with 0.1 η-units bin width can be achieved (as estimated in single central HIJING [47, 48] events).

In the following we will assume that the uncertainty on the multiplicity measurement is negligible with respect to that on the effective energy measurement.

4.2 ZDC performance for leading nucleons

As mentioned in Sect. 1, the ALICE experiment will be able to measure the energy of the leading particles needed for this study thanks to the presence of the zero degree calorimeters (ZDCs) [12]. The aim of this section is to show that this system, although designed for the detection of nearly monochromatic ($E_{\rm N} \approx 2.75$ TeV) leading nucleons in ion–ion collisions at $\sqrt{s_{\rm NN}} = 5.5$ TeV, will be able to measure on an event-by-event basis leading particles in pp collisions over a wide range of energies and with a good accuracy.

A scheme of the ZDC apparatus is shown in Fig. 7; it consists of two identical elements, placed on both sides of the interaction vertex at a distance of 115 m. Each element consists of two distinct calorimeters, one for leading neutrons (ZDCN), placed at zero degrees relative to the LHC axis, and one for leading protons (ZDCP), placed externally to the outgoing beam pipe on the side where positively charged particles are deflected by the beam optics. For charged particles, the Feynman-x range experimentally accessible with the ZDCs will be $x_{\rm F} \in [0.30–0.64]$, as the beam optics selects energies between 2.2 TeV and 4.5 TeV. For neutral particles such constraints are clearly not present. A more detailed description of the calorimeters is given in [12].

The performance of the ALICE ZDC calorimeters were first checked on single highly energetic protons and neutrons, with generated longitudinal momenta in the range between 1 TeV and 6 TeV. As mentioned before, due to the beam optics the ZDC acceptance is restricted to protons with energies in the range $2.2 < E < 4.5$ TeV, while in the case of neutrons the whole range of energy is accessible. The GEANT [49] package and the ALICE simulation and reconstruction software, AliRoot [50], were used for the simulation of the detector response, and to perform realistic digitization and reconstruction in the ZDC calorimeters.

In Fig. 8 the energy reconstructed in the ZDCs for protons and neutrons as a function of the generated energy is shown. While a good linearity is observed in the case of neutrons over the whole range of energies, in the case of protons the reconstructed energy is underestimated with respect to the true energy above ~ 3 TeV. This is because with increasing energy, the impact point of these particles falls closer and closer to the edge of the detector due to the beam optics, and the hadron cascade is no longer fully contained in the calorimeter. The energy resolution, shown in Fig. 9, ranges between 10% and 20% both in the neutron and proton cases in the selected energy range (from 2.2 to 4.5 TeV). The absolute error on the energy measurement is about 500 GeV. For protons the ZDCP energy resolution could likely be improved using the information of the impact point of the track on the calorimeter front face.

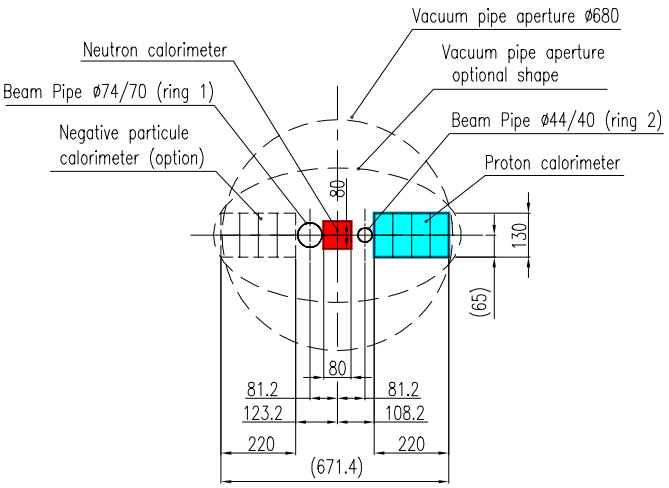

Fig. 7. Transverse section of the LHC beam line at a distance of 115 m from the interaction vertex. The location of the two ZDC calorimeters for protons and neutrons is also shown

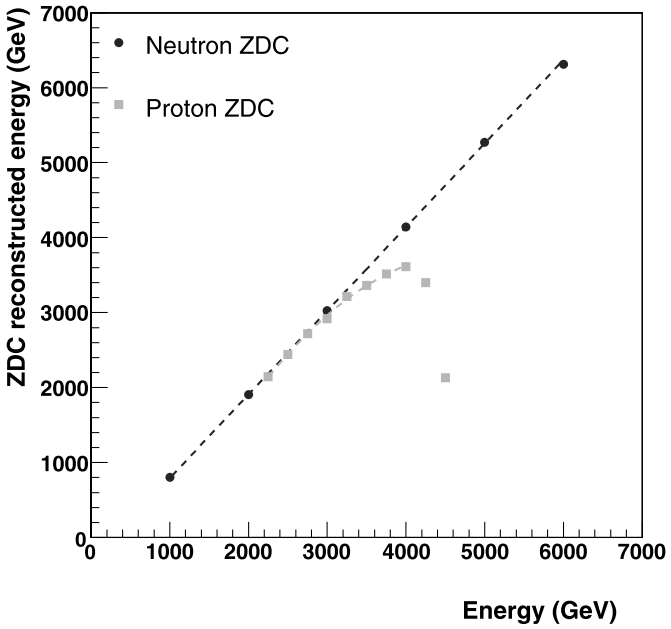

Fig. 8. Reconstructed energy in the proton (*grey symbols*) and neutron (*black symbols*) ZDC calorimeters, as a function of the proton/neutron generated energy

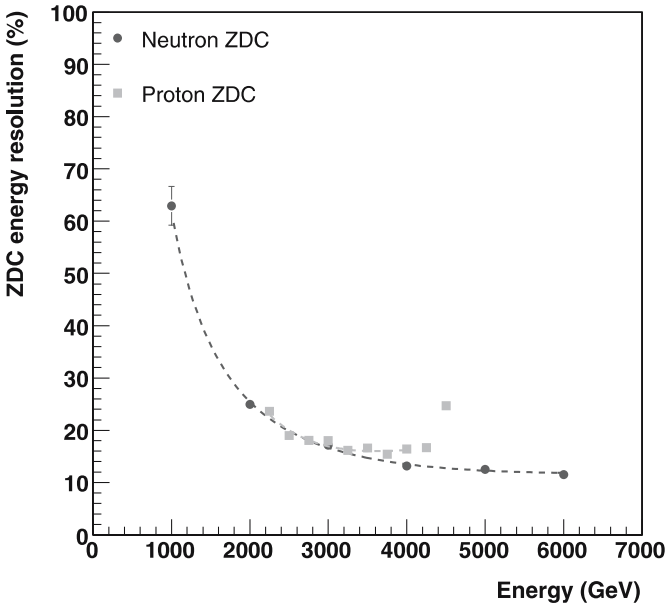

Fig. 9. Energy resolution $\delta E/E$ of the proton (*grey symbols*) and neutron (*black symbols*) ZDC calorimeters, as a function of the proton (neutron) generated energy

After checking that the ZDCs can measure the energy of forward-going nucleons over an extended $x_{\rm F}$ range, their performance has been tested on fully simulated pp collisions. Starting from 14000 generated events, in about 75% of the events a signal is recorded in either the proton (ZDCP) or the neutron (ZDCN) calorimeter, in the forward or backward regions. In the majority of cases the proton calorimeter is hit by a single particle, while in the case of the neutron calorimeter the multiplicity is higher, due to additional photons coming from the decay of high-energy forward π^0 mesons produced in the interaction (in the case of the proton calorimeter, the corresponding contamination which would be expected from charged pions is to a large extent removed by the beam optics). This is demonstrated in Fig. 10a and b, where the multiplicity of particles detected in each of the ZDC calorimeters[3] and their particle species composition are respectively shown. Moreover, looking at the fraction of deposited energy of the most energetic particle hitting the ZDCs (Fig. 11), it can be seen that in nearly all cases more than 95% of the total energy released in the ZDCP is due to a single particle, while in the ZDCN this happens only in about 50% of the cases. This is again mostly due to the background coming from photons from π^0 decays mentioned above.

The presence of additional particles impinging on the neutron calorimeter causes a substantial distorsion when the total energy measured in the calorimeter is used to estimate the energy of the leading particle entering the ZDCN, as can be seen in Fig. 12b, where the difference between the total energy measured in the ZDCN calorimeter and the generated leading particle energy is shown.

[3] In order to reject very low-energy background, only particles with Feynman-x $x_F > 0.1$ were considered.

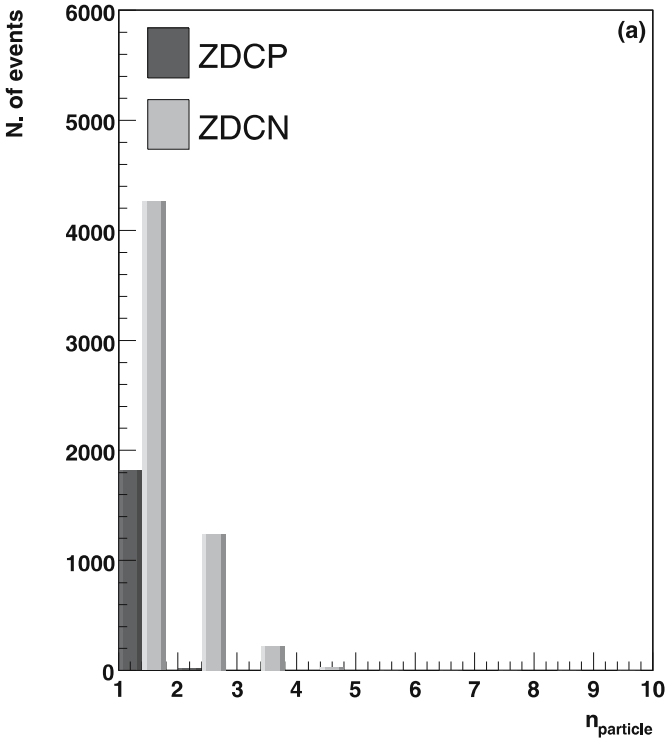

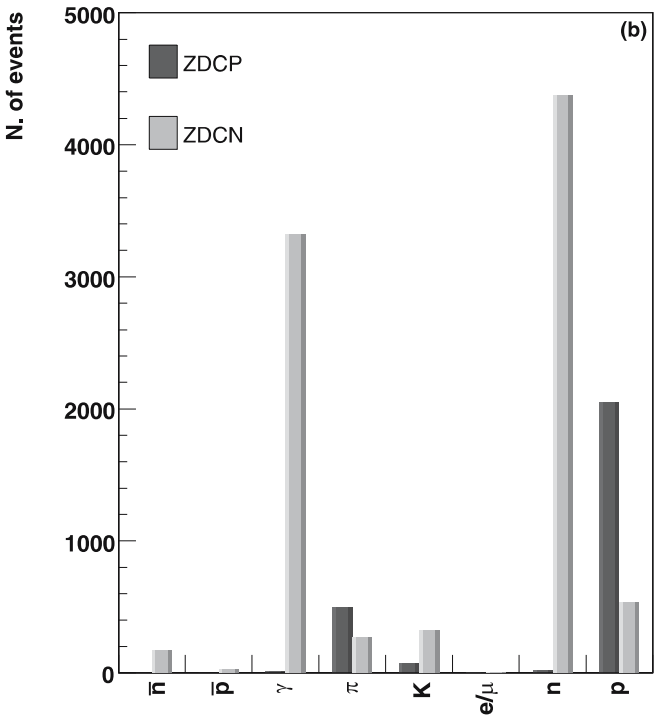

Fig. 10. Multiplicity of particles ($n_{\rm particle}$) detected in each section of the ZDC calorimeters (**a**) and the corresponding particle species composition (**b**), per single hemisphere

In the case of the proton calorimeter, where this type of background is much lower, the distribution is nearly gaussian (see Fig. 12a), although the energy is, on average, slightly underestimated due to hadronic showers not being fully contained for $E > 3$ TeV. Therefore, in terms of

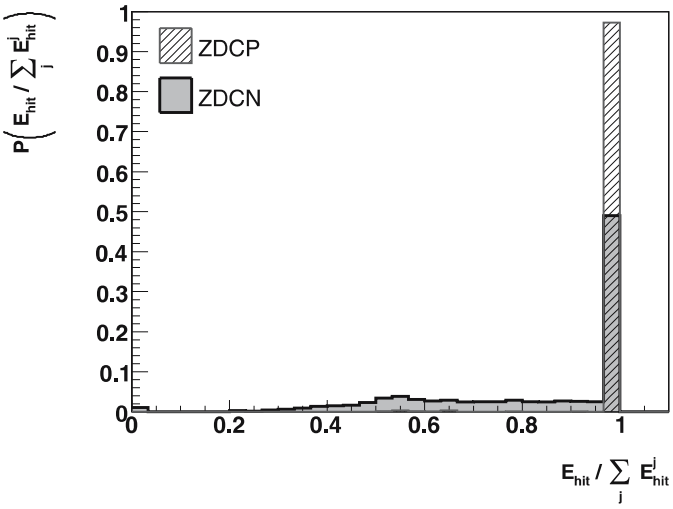

Fig. 11. Probability distribution with respect to the fraction of deposited energy of the fastest particle in the ZDCP or ZDCN

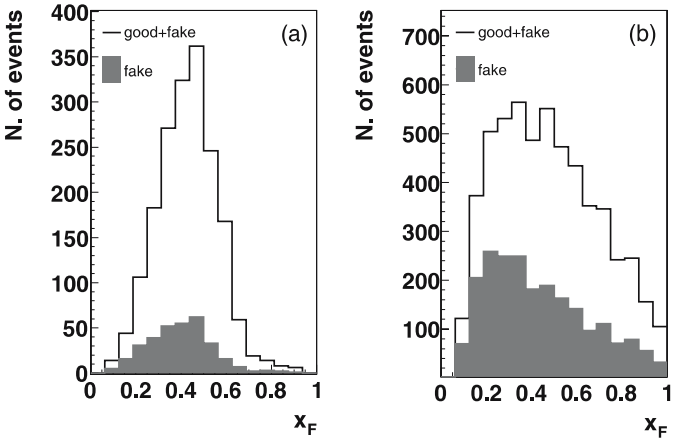

Fig. 13. Distribution of the leading Feynman–x reconstructed with the ZDCP (**a**) and ZDCN (**b**) (*empty histograms*). The contamination from the cases where the highest energy deposit in the calorimeter was not due to a leading baryon are shown as *dark shaded* histograms

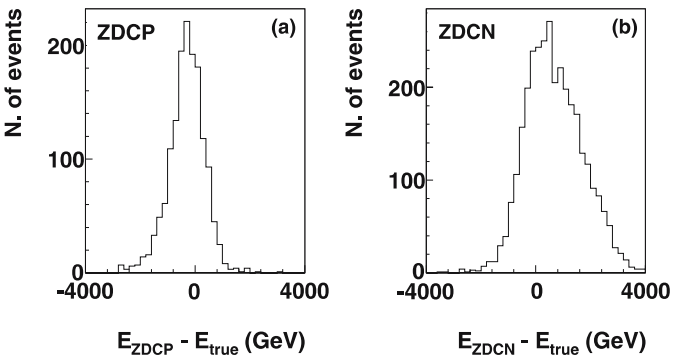

Fig. 12. Difference between the reconstructed and the generated energy in the ZDCP (**a**) and ZDCN (**b**). In the case of the ZDCN, the clear distortion on the positive side of the distribution in (**b**) is due to the presence of high energy γ's from π^0 decays, which cause an overestimate of the reconstructed energy

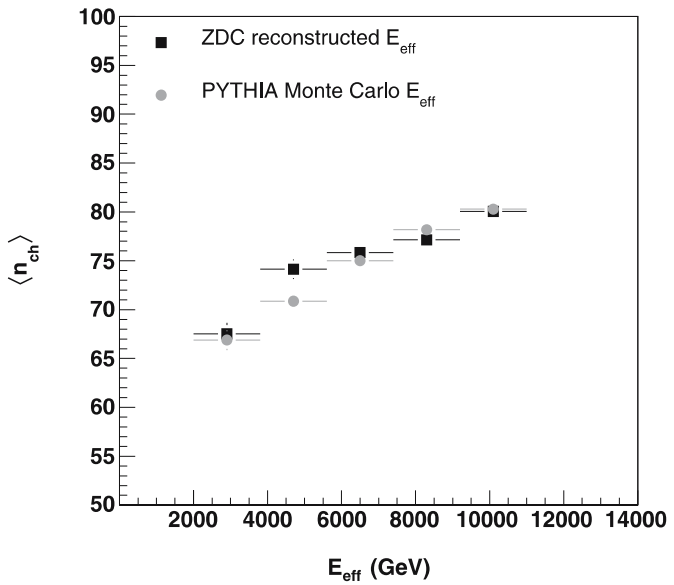

Fig. 14. Average charged multiplicity as a function of the effective energy reconstructed in the ZDC calorimeters (*black symbols*) and of the effective energy calculated at the generator level (*grey symbols*)

the effective energy reconstruction, the proton calorimeter ZDCP is expected to provide a cleaner measurement with respect to the ZDCN. On the other hand, the neutron calorimeter covers a range in Feynman-x which is more extended than in the case of the proton calorimeter, as discussed before in this section.

The reconstructed $x_{\rm F}^{\rm reco} = 2E_{\rm ZDC}/\sqrt{s}$ distribution, where $E_{\rm ZDC}$ is the total energy in either the ZDCP or the ZDCN, is shown in Fig. 13.

In those cases where a signal is detected in both calorimeters, the highest among the two energies was taken as an estimate of the leading particle energy. The empty and the dark-shaded histograms indicate respectively the Feynman-x distribution of the reconstructed leading particles and the contamination from cases where the highest energy deposit in the calorimeter was not due to a leading baryon. This latter component, which can be regarded as a source of contamination in the measurement of the effective energy, is about 30% in the case of the ZDCP and 40% in the case of the ZDCN over the Feynman-x range used in the analysis ($0.3 < x_{\rm F}^{\rm reco} < 0.8$). This contamination, however, is expected not to affect significantly the quality of the measurement of the multiplicity as a fuction of the effective energy. This is shown in Fig. 14, where the generated average charged event multiplicity as a fuction of the reconstructed effective energy $E_{\rm eff}^{\rm reco} = \sqrt{s} - 2E_{\rm ZDC}$ (black symbols), and of the effective energy calculated at the generator level (grey symbols) are compared. In both cases (2) was used. The width of the horizontal binning is determined by the energy resolution of the ZDC calorimeters.

The results are consistent, indicating that the limitations related to the reconstruction of the effective energy

in the ZDCs and the background from other particles in the forward region do not introduce a significant bias in the measurement. We therefore expect that the ALICE experiment will have a good capability to perform an effective energy study in pp collisions at LHC.

5 Nucleus–nucleus collisions

As described in the previous sections, hadron–hadron collisions produce a mean charged multiplicity in good agreement with the e^+e^- collisions at the same effective energy. Another question is still open. What happens in nucleus–nucleus? The aim of this section is to investigate the possible scenario which we expect to be observed at LHC.

The PHOBOS experiment at RHIC has recently shown (Fig. 15) how the total charged multiplicity in AA collisions, scaled by the number of participant nucleons, varies with $\sqrt{s_{\rm NN}}$ energy [51]. In particular, the AA data indicate that the scaled total charged multiplicity does not depend, to a good approximation, on the centrality of the collision and that its value vs. $\sqrt{s_{\rm NN}}$, for $20 < \sqrt{s_{\rm NN}} < 200\,\text{GeV/nucleon pair}$, is in good agreement with the one measured in e^+e^- collisions vs. $\sqrt{s}$. These findings favour the hypotesis that in AA collisions, at very high energy, $E_{\rm eff}$ would coincide with $\sqrt{s_{\rm NN}}$ for each nucleon-pair system.

Assuming that this will hold also at LHC energies, it is then possible, on the basis of an extrapolation from the e^+e^- fit, to derive a prediction for the mean total charged multiplicity per nucleon pair in nucleus–nucleus collisions at $\sqrt{s_{\rm NN}} = 5.5\,\text{TeV}$. The predicted mean total charged multiplicity, scaled by the number of participants ($N_{\rm part}$), would in fact be:

$$\frac{2}{N_{\rm part}}\langle n_{\rm ch}\rangle = 72 \pm 2\,, \tag{5}$$

resulting then in a total charged multiplicity in very central Pb–Pb collisions at the LHC (using the maximum possible value $N_{\rm part} = 416$, which is the total number of nucleons available in Pb–Pb collisions):

$$\langle n_{\rm ch}\rangle = 15000 \pm 400\,. \tag{6}$$

Once the total multiplicity is fixed, a prediction for the charged multiplicity at midrapidity (which is relevant for the measurement of a lot of observables in Pb–Pb collisions) can be derived in the so-called limiting fragmentation hypothesis. As shown in Fig. 16, several measurements from $pp(\bar{p})$ [52, 53] at different centre-of-mass energies support the fact that the multiplicity at rapidities close to the beam rapidity (the so-called fragmentation region) has a shape which is independent of the energy in the collision. This effect [54] has been observed at very different centre-of-mass energies also in DIS events. It depends only on the nature of the incident systems and, in the case of nuclei, on

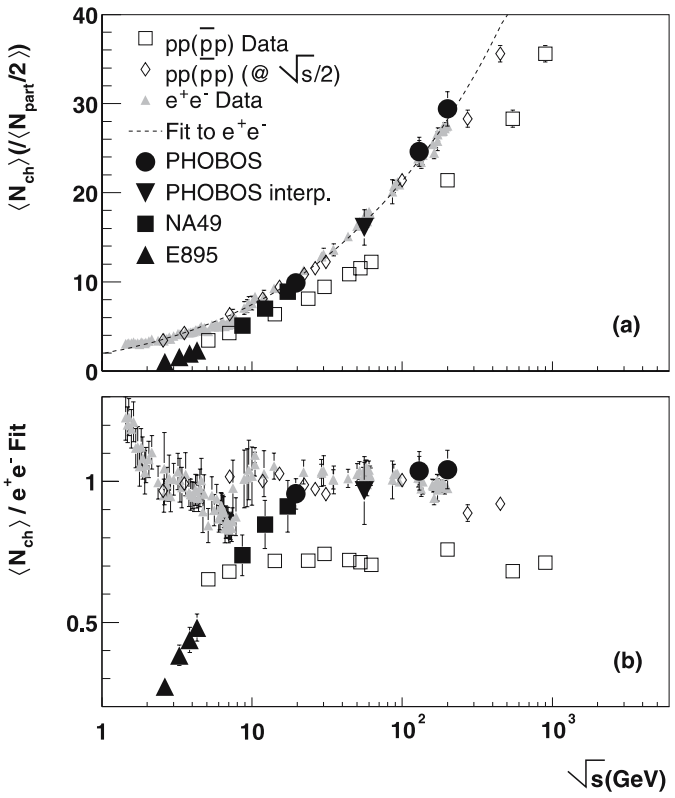

Fig. 15. a Average charged multiplicity for pp, $p\bar{p}$, e^+e^- and central Au–Au events as a function of the centre-of-mass energy per binary collision. The Au–Au (Pb–Pb for NA49 experiment) data are scaled by a factor $\langle N_{\rm part}/2\rangle$. The *dotted line* is a perturbative QCD fit to the e^+e^- data. The *diamonds* are the $pp(\bar{p})$ data plotted at energy values scaled by a factor 1/2. **b** The data in (**a**) divided by the e^+e^- fit, to allow direct comparison of different data at the same energy. Both plots (**a**) and (**b**) are taken from [51]

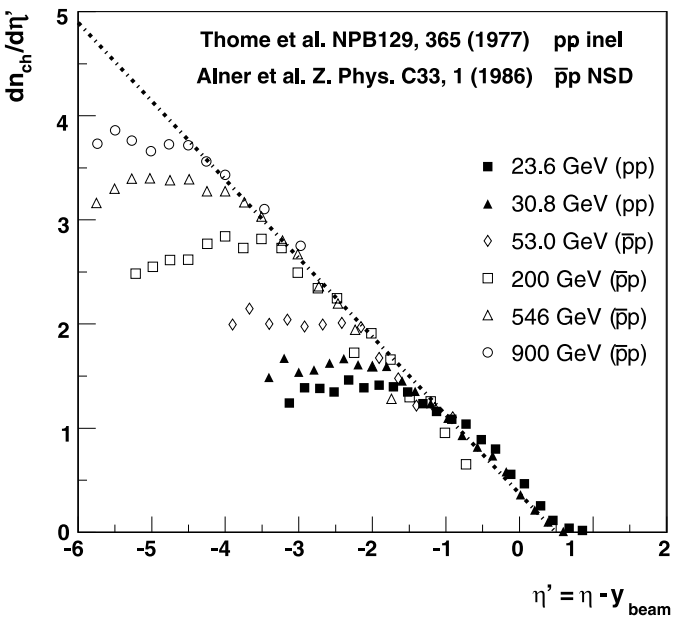

Fig. 16. Limiting fragmentation in pp and $p\bar{p}$ collisions at different centre-of-mass energies

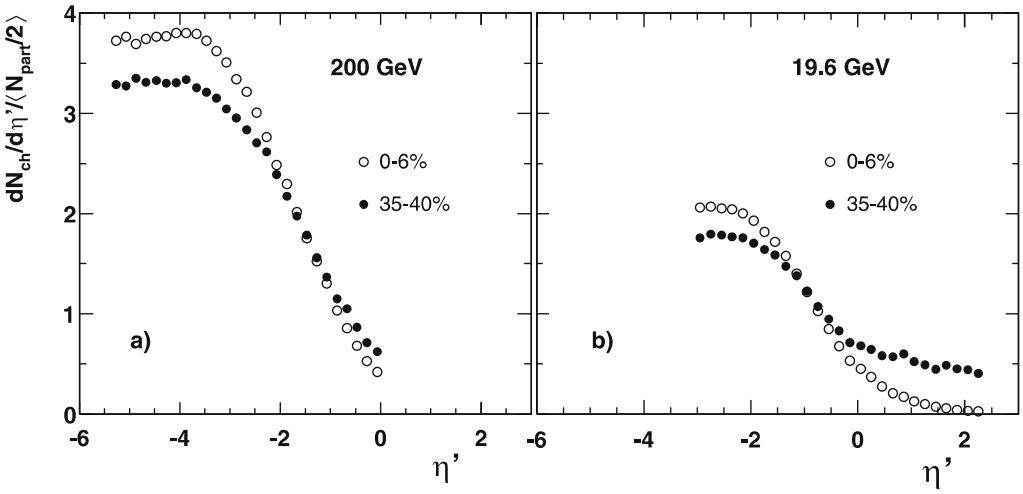

Fig. 17. PHOBOS (RHIC) results for Au–Au collisions at $\sqrt{s_{\rm NN}} = (19.6,\ 200)$ GeV. In this figure, taken from [51], the results of $\frac{2}{N_{\rm part}} \mathrm{d}N_{\rm ch}/\mathrm{d}\eta'$, where $\eta' = \eta - y_{\rm beam}$, are presented for different centrality bins

the centrality of the collision. The same behaviour is indeed preserved in AA collisions at RHIC, as shown in Fig. 17 by the measurements of the rapidity distribution for different centralities from the PHOBOS collaboration.

As shown in [52–54], the behaviour of the pseudorapidity distribution has some universal features and this allows to fix the shape of the pseudorapidity distribution *a priori*, independently of the centre-of-mass energy of the collision. Anyway such universal behaviour doesn't allow to establish the height at which the distribution is cut. This information can be found requiring that the integral under the curve should give the total charged multiplicity as predicted from the extrapolation logarithmic fit to the e^+e^- data.

Therefore, in these hypotheses it is possible to fix the shape of the pseudorapidity distribution [52–58] and derive the mean charged multiplicity at midrapidity in central Pb–Pb collisions at LHC, as it is shown in Fig. 18.

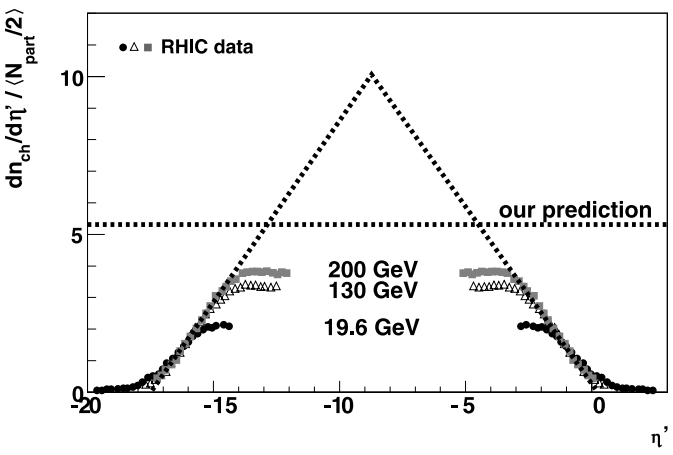

Fig. 18. Limiting fragmentation at LHC based on an extrapolation from RHIC results in central (0%–6%) ion–ion collisions. The *dashed line* indicates the value of the charged multiplicity per rapidity unit (scaled by the number of participants) which results in a total multiplicity (given by the integral under the curve) equal to the prediction from the e^+e^- fit. The rapidity of the beam at LHC is $y_{\rm beam} = 8.6$

The result is:

$$\frac{2}{N_{\rm part}} \left\langle \frac{\mathrm{d}n_{\rm ch}}{\mathrm{d}\eta} \right\rangle \Bigg|_{\eta=0} = 5.3 \pm 0.5\,, \qquad (7)$$

corresponding to about 1100 ± 100 charged tracks per rapidity unit.

There are a lot of predictions for this observable based on as many models. These models, that are compatible with the actual experimental results or are tuned on them, produce a very wide spread of predictions. In particular, a recent direct extrapolation from RHIC data seems to indicate that the charged multiplicity at LHC, in heavy ion central

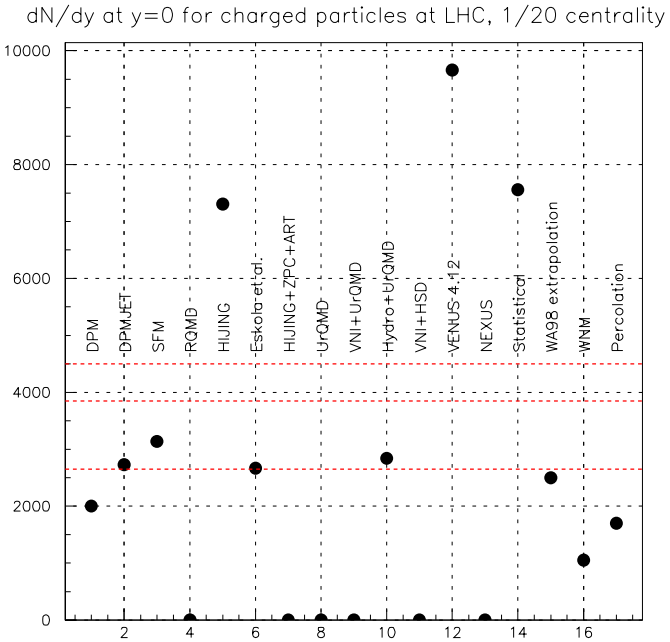

Fig. 19. Mean charged multiplicity per rapidity unit at $\eta = 0$ from different models, at $\sqrt{s_{\rm NN}} = 5.5$ TeV. For those models for which the extrapolation to LHC energies has not been performed, the corresponding value is set to zero [60]

collisions at midrapidity, could be very small ($\langle \mathrm{d}n_{\mathrm{ch}}/\mathrm{d}\eta \rangle \sim 1200$) [59], in good agreement with our prediction.

Figure 19 taken from [60] is a review of the results of the main models. It can be noted that there are predictions of over 6k charged tracks per rapidity unit and others of less than 3k.

Our prediction is significantly low when compared with the predictions of widely used Monte Carlo generators (such as HIJING, for example). It should be noted however that other effects, in particular the jet quenching [61], could sizeably increase the multiplicity in the central rapidity region. In Fig. 19 only the point relative to HIJING takes somehow into account such an effect (averaging on the two possible scenarios with and without quenching) [60]. An increase by a factor $\sim$ 2 is actually predicted by HIJING when its default[4] jet quenching algorithm is switched on. Even considering this additional effect, if the universality features hold at LHC energies, a relatively low value for the charged multiplicity at midrapidity is expected to be observed. In that case, while the physics reach of ALICE will not be endangered, as illustrated in [11] versus many representative physics observables, its background conditions would correspondingly improve.

6 Conclusions

In this work we have estimated the average charged particle multiplicity at midrapidity of the events that will be produced in Pb–Pb interactions at LHC, in an extremely high energy density domain. Our result, derived by means of detailed Monte Carlo simulations, was inspired by previous experimental findings and based on the sound hypothesis that the universality features of multihadron final states will still apply at LHC, in both *pp* and *AA* interactions.

The measurement of the leading baryons which will be needed to deduce the effective energy, e.g. the essential parameter of this analysis, has been proven to be feasible using the zero degree calorimeters (ZDCs) of the ALICE detector. We have shown, in particular, the capability of ALICE to perform an effective energy study in the range 3–10 TeV for *pp* collisions at $\sqrt{s} = 14$ TeV. This will be possible taking advantage of the acceptance and energy resolution ($\sim$ 500 GeV) of the ZDC calorimeters to measure protons and neutrons with Feynman-x $0.3 < x_{\mathrm{F}} < 0.8$.

The rather low multiplicity prediction obtained herein for large centrality Pb–Pb collisions at LHC, namely $\langle \mathrm{d}n_{\mathrm{ch}} / \mathrm{d}\eta \rangle = 1000$–$2000$ at $\eta \sim 0$ and $\sqrt{s_{\mathrm{NN}}} = 5.5$ TeV, adds to the so far uncertain mosaic of the predictions of such a very fundamental quantity for the description of *AA* phenomena.

References

1. M. Basile et al., Phys. Lett. B **92**, 367 (1980)
2. M. Basile et al., Phys. Lett. B **95**, 311 (1980)
3. M. Basile et al., Nuovo Cim. A **67**, 244 (1982)
4. M. Basile et al., Nuovo Cim. A **79**, 1 (1984)
5. M. Basile et al., Lett. Nuovo Cimento **38**, 359 (1983)
6. M. Basile et al., Nuovo Cim. A **73**, 329 (1983)
7. ALICE Collaboration, ALICE: Technical Proposal for A Large Ion Collider Experiment at the CERN LHC, CERN/LHCC 95–71 (1995)
8. ALICE Collaboration, ALICE: Technical Proposal for A Large Ion Collider Experiment at the CERN LHC (addendum 1), CERN/LHCC 96–32 (1996)
9. ALICE Collaboration, ALICE: Technical Proposal for A Large Ion Collider Experiment at the CERN LHC (addendum 2), CERN/LHCC 99–13 (1999)
10. ALICE Collaboration, F. Carminati et al., J. Phys. G **30**, 1517 (2004)
11. ALICE Collaboration, F. Carminati et al., J. Phys. G: Nucl. Part. Phys. **32**, 1295 (2006)
12. ALICE Collaboration, ALICE Technical Design Report of the Zero Degree Calorimeter (ZDC), CERN/LHCC 99–5 (1999)
13. LENA Collaboration, B. Niczyporuk et al., Z. Phys. C **9**, 1 (1981)
14. CLEO Collaboration, M.S. Alam et al., Phys. Rev. Lett. **49**, 357 (1982)
15. JADE Collaboration, W. Bartel et al., Z. Phys. C **20**, 187 (1983)
16. G.S. Abrams et al., Phys. Rev. Lett. **64**, 1334 (1990)
17. M. Derrick et al., Phys. Rev. D **34**, 3304 (1986)
18. TPC/Two Gamma Collaboration, H. Aihara et al., Phys. Lett. B **184**, 299 (1987)
19. AMY Collaboration, H.W. Zheng et al., Phys. Rev. D **42**, 737 (1990)
20. ALEPH Collaboration, R. Barate et al., Phys. Rep. **294**, 1 (1998)
21. ALEPH Collaboration, D. Buskulic et al., Z. Phys. C **73**, 409 (1997)
22. ALEPH Collaboration, Prepared for 29th International Conference on High-Energy Physics (ICHEP 98), Vancouver, British Columbia, Canada, 23–29 July 1998, CERN/OPEN 99–301
23. DELPHI Collaboration, P. Abreu et al., Eur. Phys. J. C **6**, 19 (1999)
24. L3 Collaboration, B. Adeva et al., Phys. Lett. B **259**, 199 (1991)
25. OPAL Collaboration, G. Alexander et al., Z. Phys. C **72**, 191 (1996)
26. OPAL Collaboration, K. Ackerstaff et al., Z. Phys. C **75**, 193 (1997)
27. OPAL Collaboration, G. Abbiendi et al., Eur. Phys. J. C **16**, 185 (2000) [arXiv:hep-ex/0002012]
28. OPAL Collaboration, R. Akers et al., Z. Phys. C **68**, 203 (1995)
29. http://www.slac.stanford.edu/spires/hepdata/online/ee/
30. Ames–Bologna–CERN–Dortmund–Heidelberg–Warsaw Collaboration, A. Breakstone et al., Phys. Rev. D **30**, 528 (1984)
31. M. Biyajima, T. Mizoguchi, N. Nakajima, A. Ohsawa, N. Suzuki, Phys. Lett. B **515**, 470 (2001) [arXiv:hep-ph/0106016]
32. UA5 Collaboration, G.J. Alner et al., Phys. Lett. B **138**, 304 (1984)
33. UA5 Collaboration, G.J. Alner et al., Phys. Lett. B **167**, 476 (1986)

[4] In ALICE different variants of this algorithm are presently being investigated.

34. UA5 Collaboration, G.J. Alner et al., Phys. Rep. **154**, 247 (1987)
35. UA5 Collaboration, R.E. Ansorge et al., Z. Phys. C **43**, 357 (1989)
36. T. Alexopoulos et al., Phys. Lett. B **435**, 453 (1998)
37. S.G. Matinyan, W.D. Walker, Phys. Rev. D **59**, 034 022 (1999) [arXiv:hep-ph/9801219]
38. CDF Collaboration, F. Abe et al., Phys. Rev. D **50**, 5550 (1994)
39. T. Sjostrand, S. Mrenna, P. Skands, JHEP **0605**, 026 (2006) [arXiv:hep-ph/0603175]
40. T. Nakada et al., CERN–LHCb–Note 99–028
41. CDF Collaboration, R. Field, Acta Phys. Pol. B **36**, 167 (2005)
42. A. Moraes, C. Buttar, I. Dawson, ATLAS Note ATL–PHYS–PUB–2005–007
43. D. Acosta et al., CERN–CMS–Note 2006–067
44. J. Conrad et al., ALICE–INT–2005–025
45. ALICE Collaboration, Forward Detectors: FMD, T0, V0 Technical Design Report, ALICE–DOC–2004–010
46. ALICE Collaboration, Technical Design Report of the Inner Tracking System, CERN/LHCC 99–12 (1999)
47. X.N. Wang, M. Gyulassy, Phys. Rev. D **44**, 3501 (1991)
48. X.N. Wang, M. Gyulassy, Phys. Rev. Lett. **68**, 1480 (1992)
49. R. Brun, F. Bruyant, M. Maire, A.C. McPherson, P. Zanarini, CERN–DD/EE 84–1
50. http://aliceinfo.cern.ch/Offline
51. PHOBOS Collaboration, B.B. Back et al., arXiv:nucl-ex/0301017
52. UA5 Collaboration, G.J. Alner et al., Z. Phys. C **33**, 1 (1986)
53. Aachen–CERN–Heidelberg–Munich Collaboration, W. Thome et al., Nucl. Phys. B **129**, 365 (1977)
54. J. Benecke, T.T. Chou, C.N. Yang, E. Yen, Phys. Rev. **188**, 2159 (1969)
55. B.B. Back et al., Phys. Rev. Lett. **91**, 052 303 (2003) [arXiv:nucl-ex/0210015]
56. B.B. Back et al., Nucl. Phys. A **757**, 28 (2005) [arXiv:nucl-ex/0410022]
57. G. Roland, J. Phys. G **31**, S573 (2005)
58. F. Gelis, A.M. Stasto, R. Venugopalan, Eur. Phys. J. C **48**, 489 (2006) [arXiv:hep-ph/0605087]
59. M. Lisa, AIP Conf. Proc. **828**, 226 (2006) [arXiv:nucl-ex/0512008]
60. N. Armesto, Inst. Phys. Conf. Ser. **5**, 219 (2005) [arXiv:hep-ph/0410161]
61. D. d'Enterria, AIP Conf. Proc. **806**, 252 (2006) [arXiv:nucl-ex/0510062]